

Magmatic Ni–Cu–Fe sulphide mineralization from the Halaguru area, Eastern Dharwar Craton, southern India

Sneha Raghuvanshi¹, N. V. Chalapathi Rao^{1,*}, Ajit K. Sahoo¹ and Debojit Talukdar²

¹Department of Geology, Institute of Science, Banaras Hindu University, Varanasi 221 005, India

²Geological Survey of India, Bengaluru 560 078, India

Here we report sulphide mineralization in a spinel-bearing orthopyroxene hornblendite from the Halaguru area, Eastern Dharwar Craton (EDC), southern India. The hornblendite contains approximately 3% olivine, 38% orthopyroxene, 56% amphibole and 2% oxide/sulphide phases. Petrographic and mineral chemistry studies show its formation as a result of the reaction between early formed olivine and hydrous silicate melt without any metamorphic imprint, despite its proximity to amphibolites–granulite isograd in the EDC. The sulphides comprise the disseminated form of pyrrhotite–pentlandite–chalcopyrite assemblage, which is well crystallized and the primary magmatic features are preserved as contact and granular textures. Absence of crustal xenoliths and lower SiO₂ (48 wt%), Sr (35 ppm), Pb (<5 ppm), U (<0.1 ppm) and Th (0.10 ppm) content coupled with higher Mg# (~82), Ni (700 ppm), Cr (2500 ppm) concentration in the bulk sample rules out the possibility of sulphide saturation by the addition of crustal-derived sulphur. Based on the combined textural and compositional criteria, the pyrrhotite–pentlandite–chalcopyrite assemblage is a product of the cooling and crystallization of immiscible sulphide globules. The initial high monosulphide solution, upon cooling, exsolves to pyrrhotite and pentlandite and later, at lower temperature, intermediate sulphide solid solution gives rise to chalcopyrite which is dominantly present around the edges of the pyrrhotite–pentlandite assemblage.

Keywords: Hornblendite, pyrrhotite–pentlandite–chalcopyrite assemblage, spinel, sulphide mineralization.

MAGMATIC Nickel–Copper–Platinum Group Elements (Ni–Cu–PGE) sulphide deposits are known to result from the segregation and concentration of immiscible sulphide liquid enriched in chalcophile elements that are partitioned from mafic or ultramafic magma. Many of the well-studied Ni–Cu–Fe–PGE sulphide deposits are associated with mafic–ultramafic intrusions, such as the Voisey's Bay, Canada¹, the Jinchuan Cu–Ni–PGE deposit, China²,

the J–M PGE reef in Stillwater complex, USA³ and the Noril'sk–Talnakh deposit, Siberia, Russia⁴. Magmatic sulphide deposits account for nearly 56% of nickel in the world market⁵, even though not all mafic–ultramafic intrusions are necessarily sulphide-mineralized.

Primary nickel deposits are not known from the Indian shield. However, Ni–PGE sulphides along with native gold have been reported from the Shankaraghatta ultramafic belt of the Western Dharwar Craton (WDC), southern India⁶. Sporadic occurrence of Ni in association with copper has been reported from Kaiga and Sowanhalli in the northern part of the WDC⁷. Nickel occurs in the overburden of the Sukinda chromite deposit, Singhbhum craton, eastern India, as nickeliferous limonite⁸.

Here, we report on the occurrence of primary Ni–Cu–Fe sulphides present as pentlandite–chalcopyrite–pyrrhotite assemblage in a spinel-bearing orthopyroxene hornblendite from Halaguru village, Mandya district, Karnataka, in the Eastern Dharwar Craton (EDC), southern India. This study aims to understand the origin of the sulphide assemblage and establish the mineral parageneses to constrain the timing of sulphide saturation in the host rock.

Study area

The Dharwar Craton of southern India comprises of EDC and WDC, sutured along the eastern margin of the Chitradurga schist belt⁹. The cratonization is marked by the emplacement of Closepet Granite of ca. 2513 Ma (ref. 10). A three-fold division of WDC, Central Dharwar Craton and EDC was recently proposed by Jayananda *et al.*¹¹ based on the thermal records from gneisses, granitoids and mafic dykes. The EDC has undergone low-pressure and high-temperature (andalusite–sillimanite) metamorphism. It is dominated by the Neoproterozoic granitic rocks known as Dharwar Batholith with minor Tonalite–Trondhjemitic–Granodiorite (TTGs) and thin narrow, elongated greenstone belts trending in the NNW–SSE direction in the north and N–S in the south^{12,13}. A progressive regional metamorphism from greenschist facies in the north to granulite facies in the south is well documented⁹.

*For correspondence. (e-mail: nvcrao@bhu.ac.in)

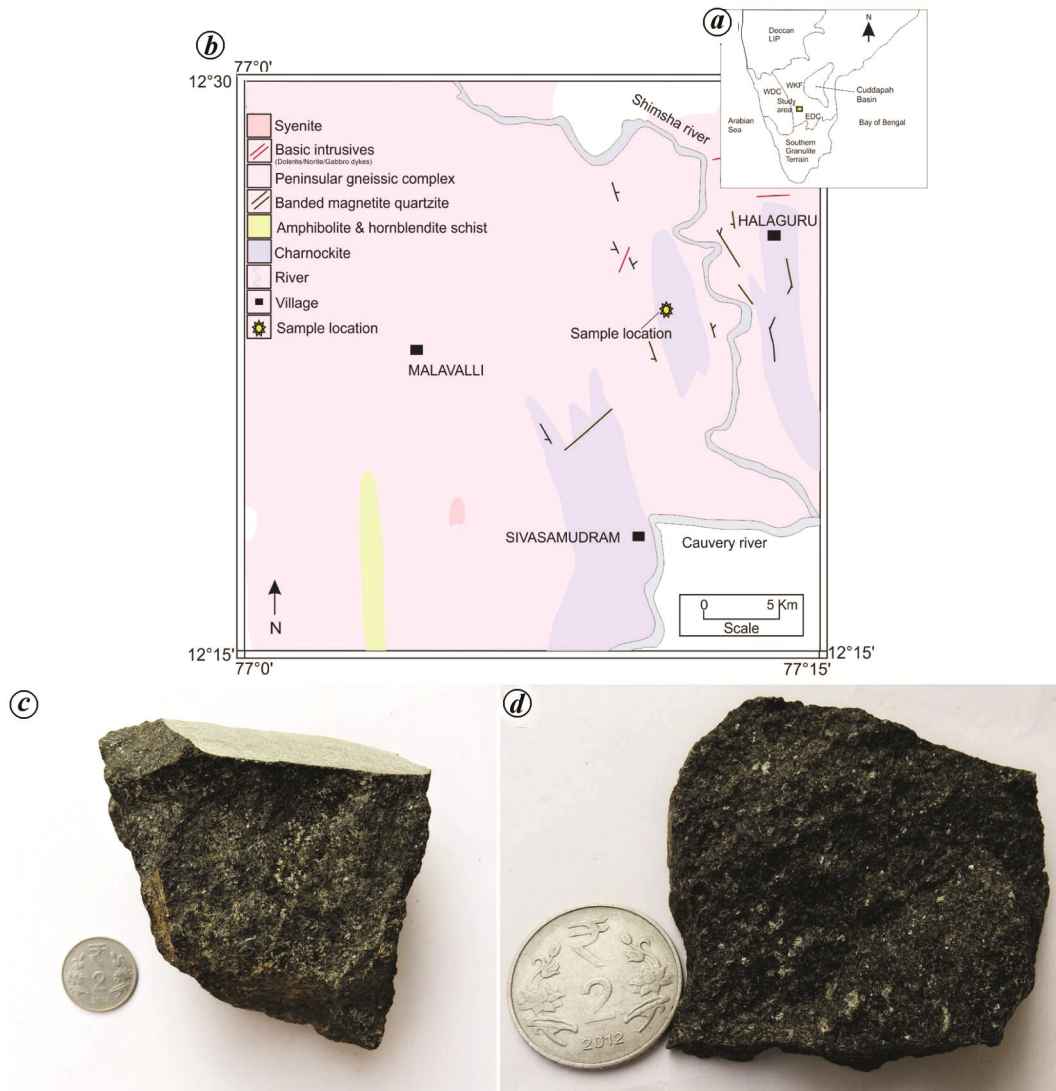


Figure 1. *a*, Generalized map of the southern Indian shield showing the location of the study area. *b*, Geological map (redrawn after Geological Survey of India¹⁴) of Halaguru area showing the sample location. *c*, *d*, Halaguru hornblendite in hand-specimen displaying (*c*) medium to coarse-grained, cumulate texture and (*d*) shiny amphibole crystals.

The Halaguru hornblendite is a small, intrusive body exposed in a pit near the TK Halli Water Treatment Plant ($12^{\circ}24'15.0984''\text{N}$, $77^{\circ}12'6.0012''\text{E}$), ~5 km south of Halaguru village (Figure 1). It is a melanocratic, shining, high-density rock composed of coarse and prismatic grains of amphibole and pyroxene. The geology of the Halaguru region comprises granitoids of the Dharwar Batholith, charnockites of the Sargur Group (Archean), syenites and basic intrusives of Proterozoic age¹⁴.

Materials and methods

Petrography of the polished thin sections was carried out using a polarizing microscope (Leica DM2700P) at the Department of Geology, Banaras Hindu University (BHU), Varanasi, India. The polished sections were coated with a

20 nm thin layer of carbon using carbon coater (LEICA-EM ACE200) for scanning electron microscopy (Carl Zeiss Evo 18 Research) and electron probe microanalysis (CAMECA-SXFive) at the Department of Geology, Banaras Hindu University (BHU), Varanasi, India. Major and minor element analyses of the minerals were carried out using CAMECA-SXFive Electron Probe Micro-analyzer (EPMA) equipped with a LaB_6 filament and five wavelength-dispersive spectrometers having LIF, PET, LPET, LTAP and PC1 crystals. The Cameca SXFive operates at a voltage of 15 kV, beam current of 10 nA, and beam diameter of 1 μm . The natural standards used for calibration of silicates were diopside (Ca), peridot (Mg), almandine (Al, Fe), orthoclase (K, Si) and albite (Na). Natural standards for sulphide calibration were pyrite (S, Fe), chalcocopyrite (Cu) and native nickel (Ni). The counting time for the major and minor elements was 10 s. The error for major

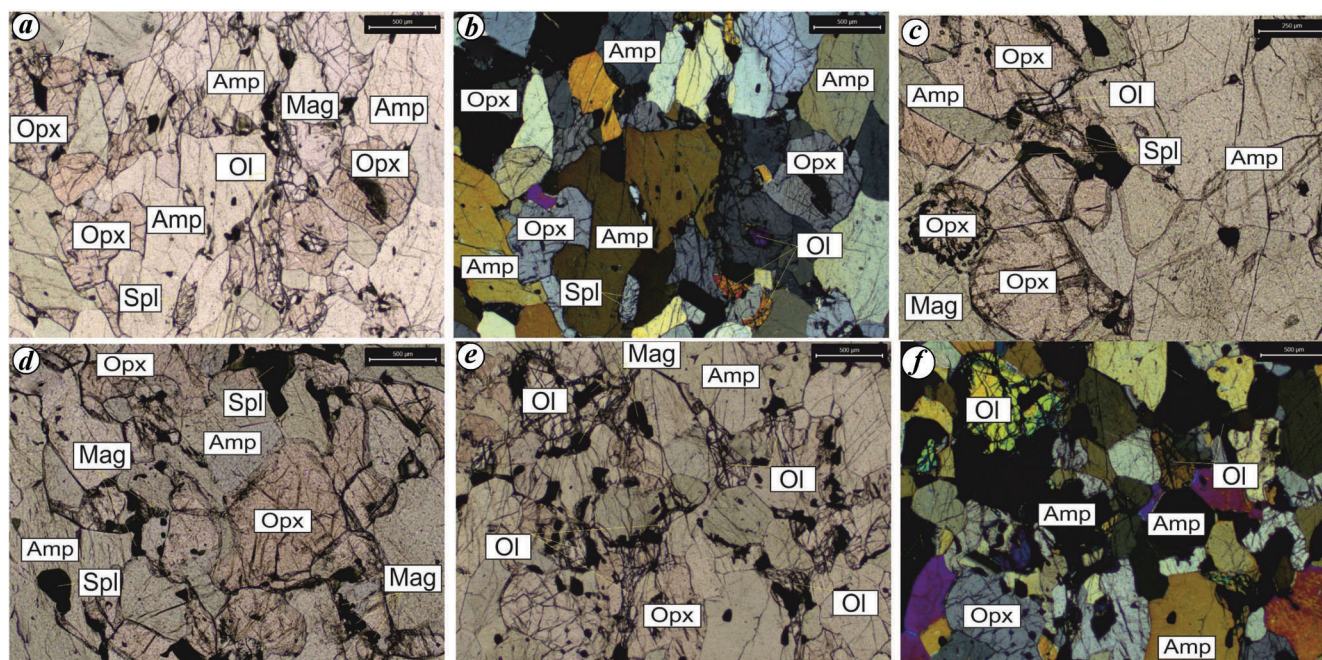


Figure 2. Photomicrographs displaying petrographic characters of silicate minerals in hornblendite in (*a, c–e*) plane-polarized light (PPL) and (*b, f*) cross-polarized light (CPL). *a, b*, Olivine (Ol), orthopyroxene (Opx) and amphibole (Amp) with sharp, straight to curved grain boundaries. Rounded relics of olivine are present in orthopyroxene. Vermicular spinels (Spl) are present in orthopyroxene from a symplectite texture. *c, d*, Rounded to vermicular magnetite (Mag) grains surrounding orthopyroxene. Spinel (Spl) have dark, turbid cores and green-coloured rims. Orthopyroxene contains small inclusions of magnetite and spinel. *e, f*, Magnetite and spinel grains tend to occur between olivine and orthopyroxene, orthopyroxene and amphibole, and amphibole and amphibole grain boundaries.

element concentration was <1% and for trace elements it varied from 3% to 5%. Representative analysis for each phase is provided in the [Supplementary Tables 1–5](#).

For whole-rock geochemistry, a fresh sample was analysed at the Activation Laboratories, Ancaster, Canada. Alkaline fusion and Inductively Coupled Plasma-Optical Emission Spectrometry (Thermo-Jarrel-Ash ENVIRO II) were used to analyse major elements and a few trace elements (V, Sc, Sr, Ba, Zr and Y). Multi-acid digestion and Inductively Coupled Plasma Mass Spectrometry (ICP-MS) analysis (Perkin Elmer Sciex ELAN 6000) were used for the measurement of trace elements concentration. STM1, MRG1, DNC1, W2 and SY3 were used as internal standards with precisions of 5% and 5%–10% for the major oxides and trace elements respectively. The bulk rock chemistry is given in [Supplementary Table 6](#).

Results

Petrography and mineral chemistry

The samples were medium-grained and showed equigranular cumulate texture. Olivine, orthopyroxene, amphibole and opaque minerals constituted approximately 3%, 38%, 56% and 2% respectively, of the area by graphical estimation using Image J software. Olivine grains occurred as inclusions within orthopyroxene (Figure 2*a*) and some grains of olivine shared mutual grain boundaries

with amphibole and orthopyroxene grains (Figure 2*e–f*). Grains of orthopyroxene and amphibole were everywhere in mutual contact with each other. Magnetite and spinel grains occurred along the intergranular spaces of silicate minerals (Figure 2*a* and *c*), near the contact between orthopyroxene and amphibole (Figure 2*c* and *d*), along fractures in olivine (Figure 2*e* and *f*) and as inclusions in silicate minerals (Figure 2*c* and *e*).

Pyrrhotite, chalcopyrite and pentlandite were the sulphide minerals distributed as disseminated aggregates (Figure 3). The sulphide aggregates exhibited (i) irregular intergrowth texture amongst pyrrhotite, chalcopyrite and pentlandite (Figure 3*d*); (ii) contact texture, wherein pentlandite occurred between pyrrhotite and chalcopyrite (Figure 3*e*) and (iii) granular texture, wherein pentlandite was associated with pyrrhotite or chalcopyrite (Figure 3*f*). These sulphide aggregates are inclusions mostly in orthopyroxene and occur in the intergranular spaces of silicates (Figure 3*b* and *c* respectively). Magnetite was the most common opaque phase followed by dark green-coloured spinel (Figure 3*d*), whereas sulphides formed only a minor component. No xenoliths or xenocrysts of the country rocks were observed.

Mineralogy of the silicates

Light green-coloured amphibole was euhedral to subhedral and displayed sharp, straight to curved boundaries with

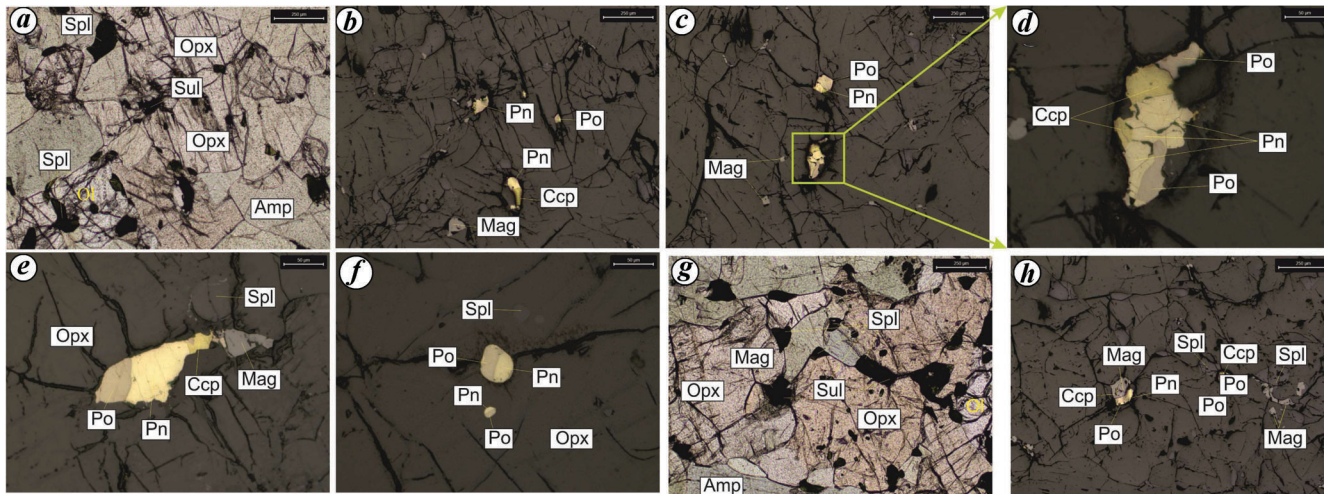


Figure 3. Photomicrographs showing textural features of sulphide ores under reflected light. *a, b*, Disseminated pyrrhotite (Po), pentlandite (Pn) and chalcopyrite (Ccp) present in the intergranular spaces between two orthopyroxene grains. *c, d*, Pyrrhotite, pentlandite and chalcopyrite showing irregular intergrowth texture. *e*, Contact texture where pentlandite is present between pyrrhotite and chalcopyrite and, (*f*) granular texture where pentlandite is associated with pyrrhotite only. *g, h*, Sulphide ores associated with magnetite and spinel, and present in the intergranular spaces of silicates.

olivine and orthopyroxene (Figure 2*a*). The absence of any reaction rim or disequilibrium texture indicates that amphibole is in textural equilibrium with olivine and orthopyroxene. Though the amphibole cores were mostly free from any inclusions, the occurrence of spinel and magnetite – along the boundaries which are in contact with olivine or orthopyroxene or both – were commonly observed (Figure 2*e*). Orthopyroxene was anhedral to subhedral and shared a curved or serrated boundary with olivine (Figure 2*a*) and a straight to the curved boundary with amphibole (Figure 2*b*). Small worm-like spinel (Figure 2*a*) and magnetite (Figure 2*c*) grains were present at the contact between orthopyroxene and amphibole as well as olivine–orthopyroxene–amphibole respectively, giving rise to symplectite texture in a few places. This may have resulted either due to the breakdown product of aluminous phases like garnet^{15–18}, or as a reaction product between olivine and hydrous silicate melt at high pressure^{19,20}. Multiple inclusions of spinel and magnetite were also present in orthopyroxene (Figure 2*c–f*). Olivine occurred as anhedral to subhedral, colourless and fractured crystals. The presence of olivine inclusions in orthopyroxene suggests that olivine is the earliest crystallizing phase. Magnetite and spinel were present as inclusions in olivine, orthopyroxene and amphibole. Magnetite was more commonly present in the fractures of olivine and in the boundaries between orthopyroxene and olivine, whereas spinel was common between the orthopyroxene and amphibole as well as amphibole and amphibole boundaries (Figure 2*e*). Rims of magnetite were present along the grain boundaries of orthopyroxene and amphibole (Figure 2*e*). Spinel was characterized by dark green turbid cores and light green rims, and present as small (~50 µm) inclusions in orthopyroxene or as larger grains (50–500 µm).

Amphibole was classified as magnesio-hornblende with a few grains sharing the boundary between magnesio-hornblende and tschermakite (Figure 4*a*), based on $Ca + Na > 1$ on B-site and $Ca_B > 1.50$ and $Na_B < 0.50$ (after Leake *et al.*²¹). They were characterized by high Mg# (0.93–0.97), displaying their magmatic nature. The average composition of orthopyroxene was $Wo_{37}En_{82.14}Fs_{17.50}$ (Figure 5)²², with a restricted range of Mg# (0.82–0.84), low Cr content (0.03–0.20 wt%) and moderate Al_2O_3 content (2–3 wt%). Olivine displayed a restricted range of Fo content (81.11–83.89%). It had high FeO (average 16 wt%), NiO (0.13–1 wt%) and MnO content (0.01–0.37 wt%). A negative correlation between Ni (wt%) and Fo content was observed in the studied sample (Figure 6), and its significance will be discussed later. The spinels were extremely rich in Al_2O_3 (47–58 wt%), MgO (9.5–15.6 wt%) and FeO (18.24–27.73 wt%) and comparatively poor in Cr_2O_3 (2.35–11.33 wt%) and hence can be termed as Al–Mg-spinels. The Cr# ($Cr/(Cr + Al)$) of the spinels ranged from 6.5 to 14. The Fe^{2+}/Fe^{3+} versus TiO_2 (wt%) ratio plot showed a high range of Fe^{2+}/Fe^{3+} ratios (Figure 7*a*). Very high Al_2O_3 (wt%) content of spinels and low TiO_2 (wt%) shows their affinity towards MORB-peridotite type of tectonic setting (Figure 7*b*). Cr_2O_3 in magnetite ranged from 2.5 to 5.8 wt% and MnO content varied from 0.03 to 0.25 wt%.

Mineralogy of the sulphides

The Halaguru hornblendite hosts a characteristic magmatic sulphide mineralogy of pyrrhotite, pentlandite and chalcopyrite. Sulphides were well crystallized, coarse (≥ 50 µm) and euhedral to anhedral in shape (Figure 3*a–f*). Pyrrhotite was the most common amongst all the three sulphides. It

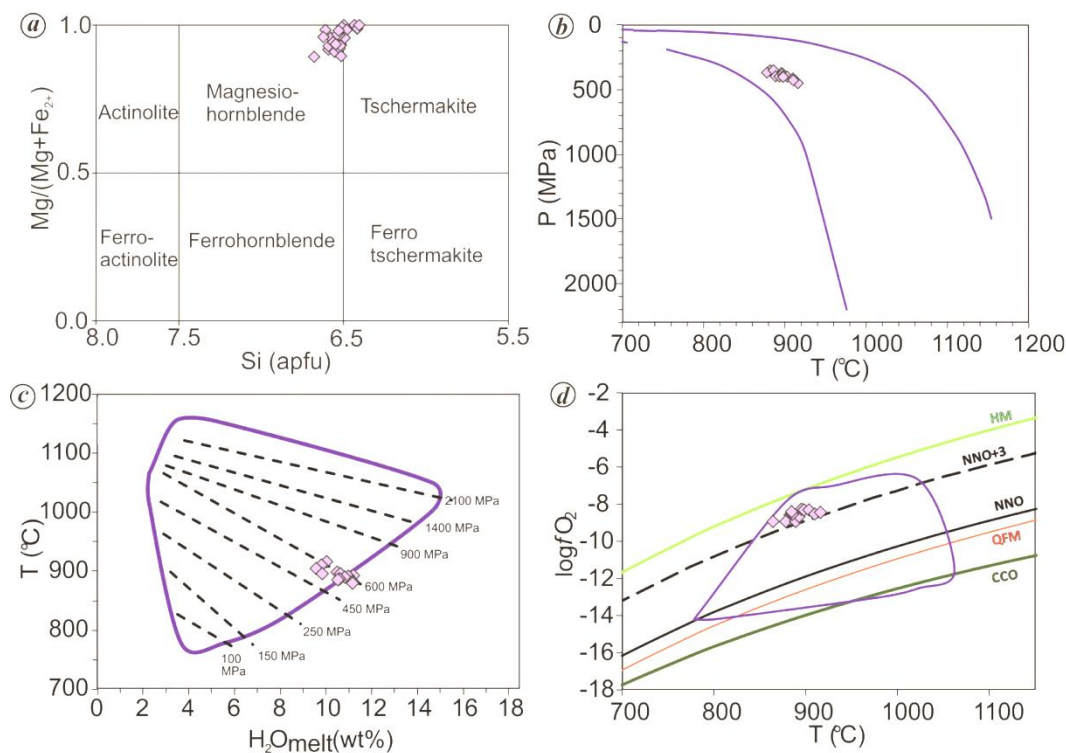


Figure 4. *a*, Si versus Mg# plot for amphibole classification from Halaguru hornblende²¹. *b–d*, Pressure, temperature, f_{O_2} and H_2O content of the melt based on the composition of amphibole in Halaguru hornblende²⁷.

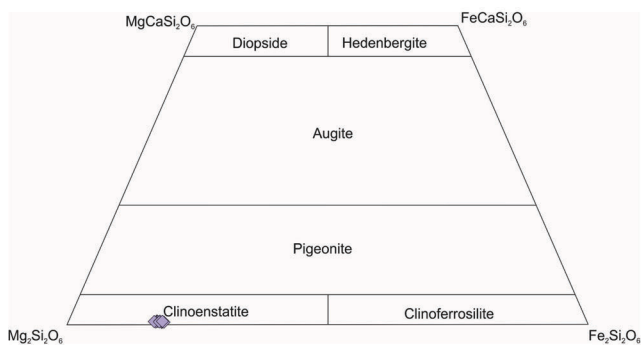


Figure 5. Pyroxene classification diagram showing enstatitic nature of orthopyroxene in Halaguru hornblende²².

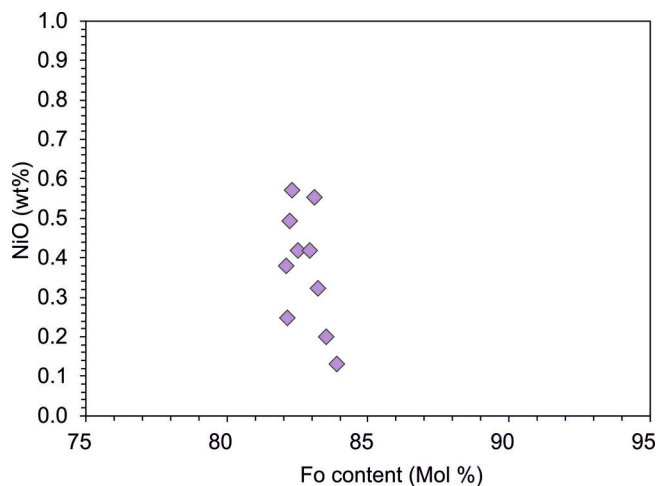


Figure 6. Decreasing Fo content with rapid increase in Ni in a plot of Ni (wt%) versus Fo content.

was typically granular and large with a pinkish-brown colour under reflected light (Figure 2 *d–e*). Pentlandite was light yellow-coloured and commonly associated with pyrrhotite and rarely with chalcopyrite (Figure 2 *b–f*). Occasionally, pentlandite occurred as discrete grains (~50 μm) with a sliver of chalcopyrite at the rim (Figure 2 *b*). Flame-shaped pentlandite commonly observed in association with pyrrhotite was absent²³. Chalcopyrite showed a dark yellow colour and occurred as anhedral grains at the outer margins of the pyrrhotite–pentlandite assemblage (Figure 2 *d*). All the sulphide minerals were homogeneous and unaltered. They showed two distinct types of

texture: (i) contact texture where pentlandite occurred between pyrrhotite and chalcopyrite (Figure 2 *e*) and (ii) granular texture where pentlandite was associated with pyrrhotite and chalcopyrite, but not with both simultaneously (Figure 2 *b* and *f*) as reported by Mansur *et al.*²⁴ from disseminated and massive sulphides of the Noril'sk–Talnakh mining district in Russia, and disseminated sulphides of the Impala Mine from Merensky Reef of the Bushveld Complex, South Africa (Figure 2 *b*).

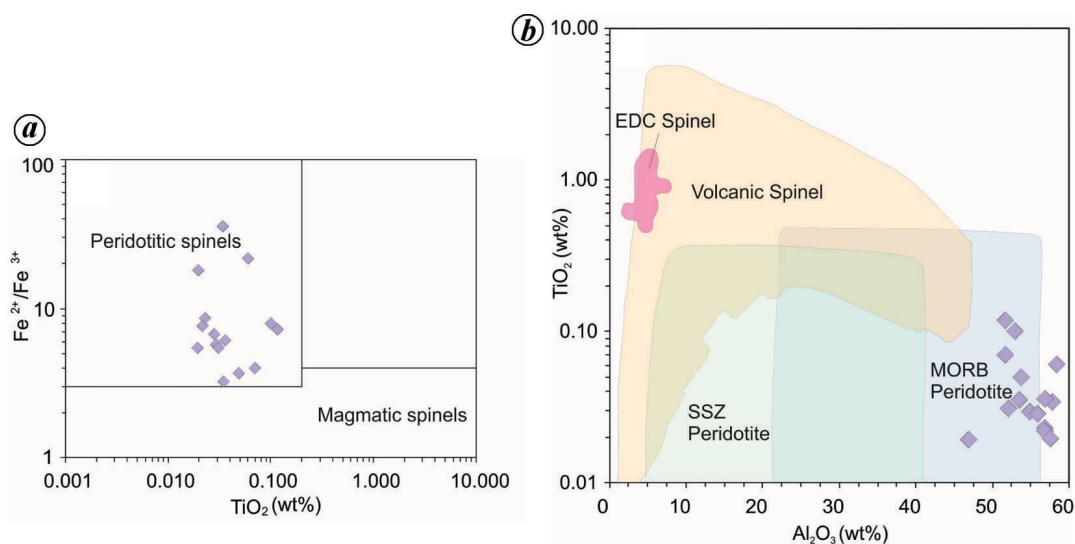
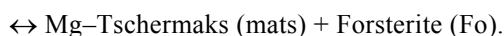
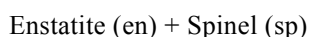


Figure 7. *a*, $\text{Fe}^{2+}/\text{Fe}^{3+}$ versus TiO_2 (wt%) for spinels in Halaguru hornblende demarcates the peridotitic and magmatic field of spinels^{33,34}. *b*, Al_2O_3 (wt%) versus TiO_2 (wt%) discrimination plot to distinguish between volcanic and mantle spinels. Fields of Eastern Dharwar Craton (EDC) spinel after Sharma *et al.*³⁵ and Giri *et al.*³⁶. Volcanic spinel, SSZ (supra-subduction zone) peridotites and MORB (mid-ocean ridge) peridotite after Kamenetsky *et al.*³⁴.

Pyrrhotite was compositionally homogenous with Ni (up to 0.70 wt%) and Co (<0.017 wt%). Pentlandite showed a wide range of Fe/Ni ratios (0.95–1.06) and had a low Co content (0.83–1.4 wt%). The Ni/(Ni + Fe) ratio in pentlandite varied from 0.49 to 0.51 wt%. Ni content in chalcopyrite was detected in small amounts (up to 0.11 wt%) and Co content was below the detection limits.

Thermobarometry

Coexisting mineral assemblages such as olivine–spinel and orthopyroxene–olivine–spinel can be used to determine the crystallization temperature of ultramafic rocks^{25,26}. Partitioning of Mg^{2+} and Fe^{2+} between $(\text{Mg}, \text{Fe}^{2+})\text{SiO}_2$ and $(\text{Mg}, \text{Fe}^{2+})(\text{Al}, \text{Cr}, \text{Fe}^{3+})_2\text{O}_4$ was first suggested by Irvine²⁷ to be useful for the estimation of crystallization temperature using an olivine–spinel thermometer. However, in Witt-Eickschen and Seck thermometry²⁶, the temperature is considered to be the function of Cr# ($\text{Cr}/(\text{Cr} + \text{Al} + \text{Fe}^{3+})$) and is based on the following equation



The occurrence of olivine in association with spinel signifies that they are in chemical equilibrium with each other. All the major cations were calculated for four pairs of olivine–spinel.

The temperature calculated for all the four mineral pairs ranged from 843°C to 1399°C (Supplementary Table 7). The large temperature range (calculated from Fabries²⁵) showed that each mineral pair reached its exchange equi-

librium at a different temperature, which was also verified by the reaction between a few spinel–olivine pairs at some places. The temperature calculated using spinel–orthopyroxene–olivine mineral assemblage (after Witt-Eickschen and Seck²⁶) ranged from 770°C to 885°C. Therefore, the overall temperature range for olivine–orthopyroxene–spinel varied from 770°C to 1399°C (Supplementary Table 7).

Amphibole can be used to determine pressure–temperature– $f\text{O}_2$ – $\text{H}_2\text{O}_{\text{melt}}$ of the magma²⁸. A single-phase thermobarometer can be used to determine temperature–pressure at which the mineral has been crystallized. Magnesio-hornblende to tschermackite type of calcic-amphiboles dominated the Halaguru hornblende. It was the last phase to crystallize among the mineral assemblage of olivine–orthopyroxene–amphibole–spinel, and its temperature and pressure were calculated to be in the range 878°C–916°C and 351–448 MPa respectively (Supplementary Table 7)²⁸. This method has an overall pressure uncertainty of $\pm 12\%$ and a temperature uncertainty of 22°C. The oxygen fugacity and $\text{H}_2\text{O}_{\text{melt}}$ varied from –7.99 to –9.05 and 9.17 to 11.91 respectively. Therefore, the depth of crystallization of amphiboles varied from 18 km to 22 km in the lower crust.

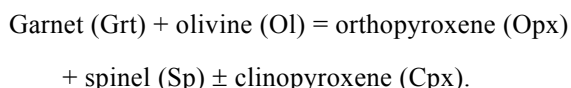
Discussion

The studied ultramafic rock could be classified as spinel-bearing orthopyroxene hornblende based on modal analysis²⁹. Although the sample was located in a charnockitic terrain, it did not show any deformation, schistosity or foliation in the hand specimen (Figure 1 *c* and *d*) or in thin sections, unlike the hornblendites of Fiskensset layered

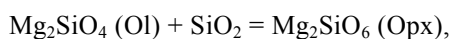
anorthosite complex, SW Greenland, which exhibited poly-deformational textures³⁰. Thus, despite the proximity of Halaguru hornblende to the amphibolite–granulite isograd in the EDC, its texture and mineral assemblage distinguished it from amphibolite to granulite facies metamorphic rocks which characterized the isograd. The hornblende–plagioclase assemblage, typical of amphibolite facies, may indicate recrystallization from magmatic precursors³⁰. However, hornblende lacks plagioclase and has a typical ultramafic assemblage similar to Gabbro Akarem, Eastern Desert, Egypt³¹. The widespread occurrence of granoblastic texture in amphiboles and the presence of magnetite grains along the grain boundaries indicate that the studied amphibole formed due to the recrystallization of a magmatic precursor. However, the sample did not contain polygonal amphibole sub-grains within amphibole to reflect metamorphic reactions and recrystallization³⁰. In fact, the textural association of amphibole–spinel, amphibole–orthopyroxene and orthopyroxene–spinel, similar to that occurring in amphibolite to granulite facies rocks formed by recrystallization³⁰ could also result from an igneous reaction between the early-formed cumulate phase and residual liquid¹⁹.

The following aspects demonstrate the formation of the Halaguru hornblende as a result of the reaction between early-formed olivine and silica-rich hydrous melt: (i) the presence of a connected network of orthopyroxene and olivine with amphibole occurring in the intergranular spaces (Figure 2 *a* and *e*), (ii) formation of magnetite at the grain boundaries of olivine–orthopyroxene and orthopyroxene–amphibole (Figure 2 *c–f*), and (iii) occurrence of symplectite along the boundary of orthopyroxene and amphibole (Figure 2 *c*).

The formation of magnetite and Al-spinel along the grain boundary of olivine and orthopyroxene may be due to the oxidation of olivine with hydrous melt acting as an oxidizing agent (Figure 2 *a* and *e*)^{19,32}. Similarly, the spinel–orthopyroxene association may result from a breakdown of garnet in the spinel stability field, represented by the following equation^{15,16}



However, most of the spinel–orthopyroxene associations were not symplectite and garnet relics or pseudomorphs were not observed in our samples, which indicates that the spinel–orthopyroxene association reported in this study cannot be explained by the breakdown of garnet. Instead, it can be the product of a reaction between early-formed olivine and residual melt rich in Si, Al and Cr. The occurrence of Al-rich spinel suggests the presence of a sufficient amount of Al in the silica-rich melt. The reactions¹⁹ can be represented as follows¹⁹



and



The composition of olivine controls the parental magma concentration, fractional crystallization, reaction with interstitial silicates and sulphide liquids, and hydrothermal alteration at elevated temperatures³³. The highly compatible nature of Ni and Mg in early-forming olivine (forsterite) decreases as crystallization proceeds. On the other hand, Fe is less compatible, and therefore, FeO/MgO ratios (i.e. the Fo content) of olivine crystallizing from the magma increase and is marked by an index of fractional crystallization. Since Ni occurs as a trace element in olivine, it tends to follow Henry's law, and its concentration will provide a guide to the concentration in the magma. The rapid decrease of Ni with Fo reflects the additional removal of Ni from the magma as it gets saturated in Ni-bearing sulphide and the sulphide droplets are removed along with mafic silicates during fractionation (Figure 6)³³.

The $\text{Fe}^{2+}/\text{Fe}^{3+}$ versus TiO_2 (wt%) plot is useful to distinguish between peridotitic and magmatic spinels (Figure 7 *a*). The high $\text{Fe}^{2+}/\text{Fe}^{3+}$ ratio shows that spinel is magmatic in origin (i.e. crystallized from the melt)^{34,35}. Due to the low diffusivity of Al, Cr and Ti cations, unlike those of Mg and Fe^{2+} in olivine, they experience the least change during post-entrapment re-equilibration. The dependence of Al_2O_3 and TiO_2 concentrations on the parental melt composition allows Al_2O_3 (wt%) versus TiO_2 (wt%) to discriminate among the spinels crystallized from different geodynamic settings (Figure 7 *b*)^{34–37}. High $\text{Fe}^{2+}/\text{Fe}^{3+} > 2$ and low $\text{TiO}_2 < 0.2$ wt% of the spinel imply their MORB-type origin.

From petrography and mineral chemistry, it can be concluded that the Halaguru hornblende results from the reaction between early-formed olivine and hydrous silicate melt. This is further evident from the formation of magnetite and Al–Mg–Fe–spinel between the fractures and intergranular spaces of olivine–orthopyroxene association due to the reaction of olivine and the liquid containing Cr, Si and Al (refs 19 and 20), and the presence of symplectite texture along the grain boundary of amphibole–orthopyroxene^{38,39}. The sudden decrease in FeO content of the magma resulted from the crystallization of magnetite and Al–Mg–Fe–spinel around the grain boundaries of early-forming minerals⁴⁰. The crystallization temperature of the olivine–orthopyroxene–spinel assemblage ranged from 1300°C to 770°C, and that of amphibole from 872°C to 936°C. The wide temperature range was due to the sub-solidus exchange of Fe–Mg between olivine and spinel during cooling. The lower limit of temperature marks the end of the Fe–Mg exchange between the olivine and spinel pair. Therefore, the temperature range of the silicates varied from 1399°C starting with olivine and ending at 872°C with amphibole, having a sub-solidus exchange reaction occurring till 780°C. The lower temperature

range of the silicates overlapped with the upper limit of crystallization temperature of sulphides at $\sim 700^\circ\text{C}$, which marks the onset of sulphide crystallization.

Evidence from textural associations

The Halaguru hornblendite consisted of a typical pyrrhotite–pentlandite–chalcopyrite assemblage and displayed a contact texture²⁴, where micrometre-sized pentlandite (Pn) grains are in contact with pyrrhotite (Po) and chalcopyrite (Ccp) grains. However, at a few places, Pn occurred independently (Figure 2 *b*) or in association with either Po or Ccp. The occurrence of typical sulphide assemblage (Po–Pn–Ccp) indicated that they were formed by cooling and crystallization of magma-derived immiscible sulphide globules (of Fe–Ni–Cu) and not by hydrothermal processes. All the grains were homogenous in composition and free from inclusions which excluded the least effect of the host rock by post-magmatic alterations.

Mechanism of metal concentration

A magmatic origin for the sulphides in this study is thus inferred from their textural features. The factors controlling sulphide solubility in the silicate melt are pressure, temperature, FeO activity in the magma, oxidation state and mafic versus felsic components of the melt⁴¹. In some of the world's most famous sulphide deposits such as the Voisey's Bay (Canada); Noril'sk–Talnakh deposits of Siberia (Russia), Merensky Reef of Bushveld Complex (South Africa) and Sudbury Ni–Cu–PGE deposits (Canada), it was found that the formation of sulphide liquid at an early stage of cooling and crystallization was not feasible and the immiscibility of sulphide liquid occurred just before emplacement of the magma⁵. Importantly, Leshar⁴² suggested that the parent magma attained sulphur saturation by digestion of high-sulphur crustal sediments or devolatilization of crustal sulphides. However, low SiO₂ (48 wt%), high MgO (23 wt%), Mg# (~ 82), Ni (700 ppm) and Cr (2500 ppm) content and low Sr (35 ppm), Pb (<5 ppm), U (<0.1 ppm) and Th (0.10 ppm) ([Supplementary Table 6](#)) coupled with the absence of any crustal xenoliths in the studied samples rule out the possibility of sulphide saturation by the addition of crustal-derived sulphur.

The Halaguru hornblendite exhibited only a small proportion ($\sim 0.5\%$) of sulphide mineralization. This indicates that the parent magma at the time of its separation from the source was sulphur undersaturated. The occurrence of sulphides in the Halaguru hornblendite was dominantly guided by the magma composition as it changed during the course of fractional crystallization, which in turn led to sulphide saturation. During the fractional crystallization of sulphur undersaturated magma, sulphur behaves as an incompatible element. Therefore, sulphur content increases as the fractional crystallization proceeds and tempera-

ture decreases^{43,44}. Sulphide saturation can be achieved as solidification proceeds and magma temperature falls with an increase in oxygen fugacity ($f\text{O}_2$) or by a decrease in the amount of ferrous iron in the magma during fractionation of the iron-rich phase. Apart from these factors, the incompatible nature of sulphur under sulphur undersaturated conditions causes its content to increase with fractional crystallization. Naldrett⁵ reported that the early crystallization of olivine was marked by a sharp fall in temperature and FeO content of the magma. With the decreasing temperature and FeO content of the magma, sulphur solubility also decreased.

In the present study, the presence of a minor amount of olivine in comparison with orthopyroxene and amphibole may be due to its early crystallization and subsequent separation from the magma. Liu *et al.*⁴⁴ have shown that the magma with calcium-rich minerals requires higher sulphur content to reach sulphide saturation. The Halaguru hornblendite mainly has olivine and orthopyroxene which contain minor amounts of calcium, and thus supports sulphide saturation. Also, the reaction between olivine and hydrous silicate melt resulted in the reduction of FeO content of the magma caused by the crystallization of magnetite and spinel present along the grain boundaries and surrounding the silicate minerals like magnetite grains rimming orthopyroxene (Figure 2 *c*), symplectite present between the amphibole and orthopyroxene as well as the amphibole–amphibole boundaries (Figure 2 *a* and *d*). Removal of FeO from magma will help it attain saturation and subsequent formation of small sulphide globules in the form of monosulphide solid solution. Sulphide globules partition all the chalcophile elements (Ni, Cu and PGE) from the ultramafic silicate portion and form an initial high-temperature phase called the monosulphide solid solution below 1100°C (refs 23 and 43), leaving a Cu-rich sulphide liquid. As the crystallization proceeds to below 900°C , Cu-rich sulphide liquid crystallizes to form intermediate sulphide solid solution^{23,43,45}. This monosulphide solid solution, upon cooling below 700°C , is no longer stable and exsolves into pyrrhotite and pentlandite, while the intermediate sulphide solid solution exsolves into chalcopyrite. The coarse and granular nature of pentlandite (Figure 2 *d* and *e*) shows that it exsolves at high temperature (650°C) and has more time to form than those grains which exsolve as veins ($T - 400^\circ\text{C}$) or flames ($T - 200^\circ\text{C}$)²⁴.

The absence of contact-zoning or antithetical zoning in pentlandite–pyrrhotite association rules out their genesis by peritectic reaction between monosulphide solid solution and fractionated sulphide liquid^{5,24}. Based on the textural study of sulphide and silicate phases of the Halaguru hornblendite, a mineral paragenetic sequence is presented (Figure 8). A detailed geological and geophysical study is needed in this domain to establish the lateral and vertical continuity of this ore body and to evaluate its economic significance.

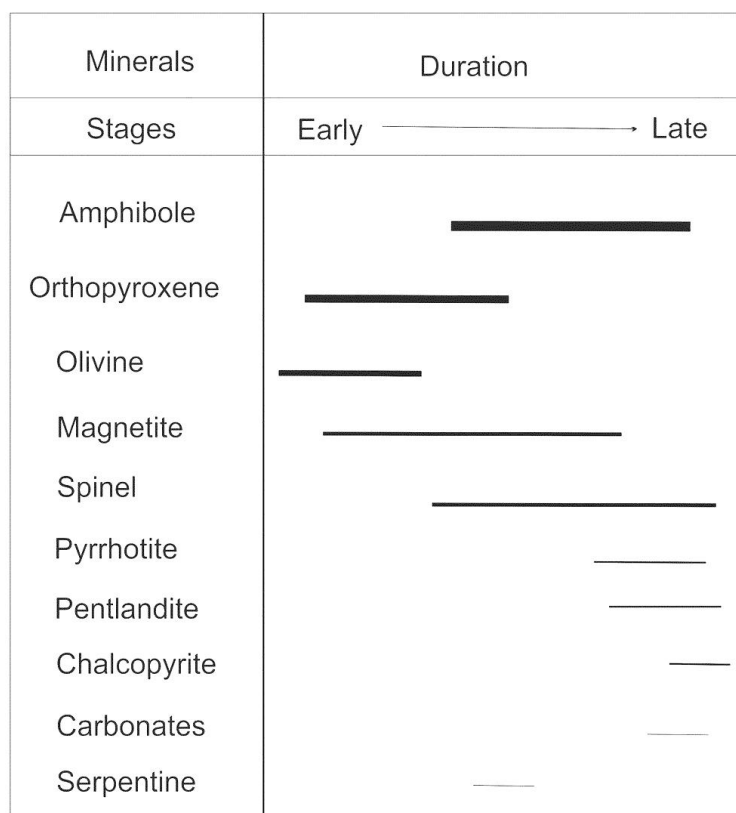


Figure 8. Schematic diagram showing the mineral paragenesis in Halaguru hornblendite. The thickness of the lines indicates relative abundance of the respective mineral.

Conclusion

Modal mineralogical composition of the Halaguru ultramafic rock classifies it as spinel-bearing orthopyroxene hornblendite containing pentlandite–chalcopyrite–pyrrhotite assemblage. Textural and mineral chemistry reveals that hornblendite was formed as a result of the reaction between early-formed olivine and hydrous silicate melt and is magmatic in origin without any metamorphic imprint. Extraction of iron-rich phase, and not saturation by crustal material, is considered the main factor controlling sulphide saturation leading to the formation of immiscible sulphide globules containing the pentlandite–chalcopyrite–pyrrhotite-assemblage. The initial high monosulphide solution, upon cooling, exsolves to pyrrhotite and pentlandite, and subsequently, at a lower temperature, intermediate sulphide solid solution gives rise to chalcopyrite.

Conflict of interest: The authors declare no conflict of interest.

1. Lightfoot, P. C. and Naldrett, A. J., Geological and geochemical relationships in the Voisey's Bay Intrusion, Nain Plutonic Suite, Labrador, Canada. In *Dynamic Processes in Magmatic Ore Deposits and their Application in Mineral Exploration*, Geological Association of Canada (eds Keays, R. R. et al.), Short Course Notes, 1999, vol. 13, pp. 1–30.

2. Yang, S. et al., Pt–Os isotopic constrains on the age of hydrothermal overprinting on the Jinchuan Ni–Cu–PGE deposits, China. *Miner. Deposita*, 2018, **53**, 757–774.
3. Barnes, S. J. and Naldrett, A. J., Geochemistry of J–M reef of the Stillwater Complex, Minneapolis adit area II. Silicate mineral chemistry and petrogenesis. *J. Petrol.*, 1986, **27**(4), 791–825.
4. Naldrett, A. J. et al., Controls on the composition of Ni–Cu sulphide deposits as illustrated by those at Noril'sk, Siberia. *Econ. Geol.*, 1996, **91**, 751–773.
5. Naldrett, A. J., *Magmatic Sulphide Deposits: Geology, Geochemistry and Exploration*. Oxford University Press, New York, USA, 2004, pp. 30–35.
6. Datta, P. et al., Origin of Ni–Cu–(PGE + Au) sulphides in late-Archean komatiitic suite of rocks in the Shankaraghatta belt, Western Dharwar Craton (India). *Ore Geol. Rev.*, 2021, **138**, 104375.
7. Radhakrishna, B. P., *Mineral Resources of Karnataka*, Geological Society of India, Bangalore, 1996, pp. 411–412.
8. Anand Rao, K. et al., Preconcentration of nickel values from lateritic chromite ore overburden, Sukinda, Orissa, India. *Miner. Process. Extr. Metall. Rev.*, 1995, **15**, 37–45.
9. Ramakrishnan, M. and Vaidyanadhan, R., *Geology of India*, Geological Society of India, Bangalore, 2008, vol. 1, p. 556.
10. Friend, C. R. L. and Nutman, A. P., SHRIMP U–Pb geochronology of the Closepet granite and Peninsular gneiss, Karnataka, South India. *J. Geol. Soc. India*, 1991, **38**, 357–368.
11. Jayananda, M. et al., Formation of Archean crust in the Dharwar Craton, southern India. *Earth Sci. Rev.*, 2018, **181**, 12–42.
12. Chadwick, B. et al., The Dharwar craton, southern India, interpreted as the result of Late Archean oblique convergence. *Precambrian Res.*, 2000, **99**, 91–111.

13. Jayananda, M. *et al.*, Late Archean (2550–2520 Ma) juvenile magmatism in the Eastern Dharwar Craton, southern India: constraints from geochronology, Nd–Sr isotopes and whole-rock geochemistry. *Precambrian Res.*, 2000, **99**, 225–254.
14. Balachandra, V. and Nagaraja Rao, K. N., *District Resources Map of Mandya district, Karnataka*, Geological Survey of India, 1991.
15. Smith, D., The origin and interpretation of spinel–pyroxene clusters in peridotite. *J. Geol.*, 1977, **85**, 476–482.
16. Field, S. W. and Haggerty, S. E., Symplectites in upper mantle peridotites: development and implications for the growth of subsolidus garnet, pyroxene and spinel. *Contrib. Mineral. Petrol.*, 1994, **118**, 138–156.
17. Morishita, T. and Arai, S., Evolution of spinel–pyroxene symplectite in spinel–lherzolite from the Horoman complex, Japan. *Contrib. Mineral. Petrol.*, 2003, **144**, 509–522.
18. Griffin, W. L. *et al.*, Mantle recycling: transition zone metamorphism of Tibetan ophiolitic peridotites and its tectonic implications. *J. Petrol.*, 2016, **57**, 655–684.
19. Jing, J.-J. *et al.*, reactive origin of mantle harzburgite: evidence from orthopyroxene–spinel association. *Lithos*, 2019, **342–343**, 175–186.
20. Johan, Z. *et al.*, Fluids are bound to be involved in the formation of ophiolitic chromite deposits. *Eur. J. Mineral.*, 2017, **29**, 543–555.
21. Leake, B. E. *et al.*, Nomenclature of amphiboles: report of the subcommittee on Amphiboles of the International Mineralogical Association, Commission on New Minerals and Mineral Names. *Mineral. Mag.*, 1997, **35**, 219–246.
22. Morimoto *et al.*, Nomenclature of pyroxenes. *Mineral. Mag.*, 1988, **52**, 535–550.
23. Craig, J. R. and Vaughan, D. J., *Ore Microscopy and Ore Petrography*, John Wiley, New York, 1994, 2nd edn, p. 215.
24. Mansur, E. T. *et al.*, Textural and compositional evidence for the formation of pentlandite via peritectic reaction: implications for the distribution of highly siderophile elements. *Geology*, 2019, **47**, 351–354.
25. Fabries, J., Spinel–olivine geothermometry in peridotites from ultramafic complexes. *Contrib. Mineral. Petrol.*, 1979, **69**, 329–336.
26. Witt-Eickchen, G. *et al.*, Solubility of Ca and Al in orthopyroxene from spinel peridotite: an improved version of an empirical geothermometer. *Contrib. Mineral. Petrol.*, 1991, **106**, 431–439.
27. Irvine, T. N., Chromian spinel as petrogenetic indicator. *Part 1. Theory. Can. J. Earth Sci.*, 1965, **2**, 648–672.
28. Ridolfi, F., Amp-TB2: an updated model for calcic amphibole thermobarometry. *Minerals*, 2021, **11**, 324.
29. Le Maitre, R. W. *et al.*, In *Igneous Rocks: A Classification and Glossary of Terms*, Cambridge University Press, UK, 2004, pp. 25–28.
30. Polat, A. *et al.*, Geochemistry of ultramafic rocks and hornblende veins in the Fiskensæset layered anorthosite complex, SW Greenland: evidence for hydrous upper mantle in the Archean. *Precambrian Res.*, 2012, **214–215**, 124–153.
31. Helmy, H. M. and Mogessie, A., Gabbro Akarem, Eastern Desert, Egypt: Cu–Ni–PGE mineralization in a concentrically zoned mafic-ultramafic complex. *Miner. Deposita*, 2001, **36**, 58–71.
32. Wang, C. *et al.*, Formation of orthopyroxenite by reaction between peridotite and hydrous basaltic melt: an experimental study. *Contrib. Mineral. Petrol.*, 2016, **171**, 77.
33. Li, C. *et al.*, Controls on the Fo and Ni contents of olivine in sulphide-bearing mafic/ultramafic intrusions: principles, modelling and examples from Voisey’s Bay. *Earth Sci. Front.*, 2007, **14**, 177–185.
34. Kamenetsky, V. S. *et al.*, Factors controlling chemistry of magmatic spinel: an empirical study of associated olivine, Cr-spinel and melt inclusions from primitive rocks. *J. Petrol.*, 2001, **42**, 655–671.
35. Sharma, A. *et al.*, Arc-related pyroxenites derived from a long-lived Neoproterozoic subduction system at the southwest margin of the eastern Dharwar Craton, southern India. *J. Geol.*, 2019, **127**, 5.
36. Giri, R. K. *et al.*, Pyroxenite dykes with petrological and geochemical affinities to the Alaskan-type ultramafics at the north-western margin of the Cuddapah basin, Dharwar craton, southern India: tectonomagmatic implications. *J. Earth Syst. Sci.*, 2019, **128**, 114.
37. Lenaz, D. *et al.*, Restitic or not? Insights from trace elements content and crystal-structure of spinels in African mantle xenoliths. *Lithos*, 2017, **278–281**, 464–476.
38. Holness, M. B. *et al.*, Silicate liquid immiscibility within the crystal mush: late-stage magmatic microstructures in the Skaergaard Intrusion, East Greenland. *J. Petrol.*, 2009, **52**, 175–222.
39. Keevil, H. A. *et al.*, Microstructure and late-stage magmatic processes in layered mafic intrusions: symplectites from the Sept Îles Intrusion, Quebec, Canada. *J. Petrol.*, 2020, **61**, 7.
40. De Angelis, S. H. *et al.*, Amphibole reaction rims as a record of pre-eruptive magmatic heating: an experimental approach. *Earth Planet. Sci. Lett.*, 2015, **426**, 235–245.
41. MacLean, W. H., Liquidus phase relations in the FeS–FeO–Fe₃O–SiO₂ systems and their application in geology. *Econ. Geol.*, 1969, **64**, 865–884.
42. Leshner, C. M., Komatiite-associated nickel sulphide deposits. *Rev. Econ. Geol.*, 1989, **4**, 44–101.
43. Barnes, S. J. *et al.*, Magmatic sulphide ore deposits. *Elements*, 2017, **17**, 89–95.
44. Liu, Y. G. *et al.*, Sulphide saturation mechanism of the Poyi magmatic Cu–Ni sulphide deposit in Beishan, Xinjiang, Northwest China. *Ore Geol. Rev.*, 2017, **91**, 419–431.
45. Barnes, S. J. and Lightfoot, P. C., Formation of magmatic nickel–sulphide ore deposits and processes affecting their copper and platinum-group element contents. *Econ. Geol.*, 2005, **100**, 179.

ACKNOWLEDGEMENTS. We thank the Head, Department of Geology, BHU, Varanasi, for support. N.V.C.R. thanks DST-SERB for sanctioning a project (IR/S4/ESF-18/2011 dated 12 November 2013) to study the lithospheric evolution beneath the Indian shield and BHU for awarding him a faculty incentive grant. S.R. thanks University Grants Commission, New Delhi (421/(CSIR-UGC NET JUNE 2018)) for a Senior Research Fellowship. Constructive suggestions by an anonymous reviewer and editorial handling by Somnath Dasgupta are acknowledged.

Received 5 December 2021; revised accepted 18 March 2022

doi: 10.18520/cs/v122/i11/1288-1297